JOURNAL OF MATERIALS SCIENCE 12 (1977) 1307–1319

Generalized fracture mechanics

Part 3 *Prediction of fracture energies in highly extensible solids*

E. H. ANDREWS, Y. FUKAHORI
Department of Materials, Queen Mary College, London, UK

According to Andrews' generalized fracture mechanics theory [1], the fracture energy of a solid is given by

$$\mathcal{T} = \mathcal{T}_0 \Phi$$

where $\mathcal{T}_0$ is a surface energy and Φ a loss function whose form is explicit. The loss function has been evaluated experimentally for four highly extensible materials, styrene–butadiene rubber, ethylene–propylene rubber, plasticized PVC and polyethylene and at various rates of crack propagation. The quantity $\mathcal{T}_0$ has also been calculated from existing theory and a prediction thus obtained for fracture energy. The results indicate good agreement between experiment and theory and thus appear to corroborate the generalized formulation of fracture mechanics in its application to non-linear inelastic materials.

1 Introduction

Previous papers in this series have dealt respectively with the basic generalized theory [1] and its application to the fracture of ductile metal alloys [2]. The investigation reported here provides a critical test of one of the most important predictions of the theory, namely that the fracture energy $\mathcal{T}$ of a solid (referred to unit area of crack interface) is given by

$$\mathcal{T} = \mathcal{T}_0 \Phi(\dot{c}, T, \epsilon_0) \quad (1)$$

where $\mathcal{T}_0$ is the energy to rupture unit area of inter-atomic bonds across the fracture plane (the 'surface energy' of the solid on one definition) and Φ is a loss function dependent on the crack velocity $\dot{c}$, the temperature T and the applied strain ϵ_0. Specifically, from consideration of an edge crack in a semi-infinite sheet,

$$\Phi = k_1(\epsilon_0) \Big/ \left[k_1(\epsilon_0) - \tfrac{1}{2} \sum_{\mathrm{PU}} \beta g \, \delta x \, \delta y \right]^* \quad (2)$$

where

$$k_1(\epsilon_0) = \tfrac{1}{2} \sum_{\mathrm{P}} q g \, \delta x \, \delta y^*, \quad (3)$$

$$g(x, y, \epsilon_0) = \left[x \frac{\partial f}{\partial x} + y \frac{\partial f}{\partial y} \right], \quad (4)$$

$$f(x, y, \epsilon_0) = W(\mathrm{P})/W_0. \quad (5)$$

$W(\mathrm{P})$ is the input energy density at a point P in the stress field, W_0 is the input energy density at points remote from the crack, x, y are the reduced cartesian co-ordinates of the point P ($x = X/c$; $y = Y/c$), c is the crack length. $\beta(x, y)$ is the hysteresis ratio at the point P, and the symbols P, PU denote summation over all points in the stress field, and over points which unload as the crack propagates, respectively. q is a negative constant of value -1 for linear materials [2].

If the energy density distribution around a crack is known, the function g, and thence k_1,

*The factor $\frac{1}{2}$ appears instead of $\frac{1}{4}$ as in [1] because we refer here to an edge crack in a semi-infinite sheet in which summations are taken only over the semi-infinite half-plane rather than the full plane considered in [1].

can be evaluated. Alternatively k_1 can be obtained directly by the compliance method described in [2]. The evaluation of the term $\sum_{PU}$ requires additionally a knowledge of the hysteresis ratio β from point to point in the stress field and β will in general be a function of the local strain, strain rate and temperature. Indeed, β will also in general depend on the amount of crack growth, Δc, since the fractional energy loss at P will depend on the degree of relaxation permitted to occur there (This effect gives rise to the phenomenon of fatigue). However, for steady state tearing (constant crack speed) as observed in the work here reported it is appropriate to use the hysteresis ratio for a full loading/unloading stress cycle at the appropriate strain rate and peak strain for β. We have not attempted, at this stage, to measure β for our materials in biaxial strain as is strictly necessary to characterize losses in the strain field around a crack. We have assumed that β is a unique function of input energy density (at a given strain rate) regardless of the strain tensor giving rise to this density and have then employed values of β derived from uniaxial tests.

To complete the theoretical evaluation of $\mathcal{T}$ from Equation 1 requires a knowledge of $\mathcal{T}_0$. This parameter may be measured by fatigue experiments in which $\mathcal{T}_0$ is the threshold energy release rate below which no growth of a crack occurs (except by chemical attack), and such measurements for one of our materials (SBR) are to be found in the literature [3, 4]. These measurements are difficult, however, and do not always succeed. An alternative approach is to caluclate $\mathcal{T}_0$ by the method of Lake and Thomas [5] which is applicable to cross-linked elastomers. Calculated values for $\mathcal{T}_0$ are typically smaller than measured values by a factor of 2 or even more. In the present work $\mathcal{T}_0$ has been calculated for all four materials used using a modified form of the theory in the case of non-cross-linked materials.

To summarize, therefore, the following measurements and calculations have been carried out in order to test the validity of Equation 1:

(a) Direct measurement of fracture energy $\mathcal{T}$.
(b) Evaluation of $k_1(\epsilon_0)$ by the compliance method.
(c) Experimental determination of strain, and thence energy, distributions around cracks and the evaluation of the function g.
(d) Experimental determination of $\beta(\epsilon, \dot{\epsilon})$.
(e) Calculation of $\mathcal{T}_0$.
(f) From (b) – (e), the calculation of a theoretical value for $\mathcal{T}$ from Equation 1 to compare with the experimental value.

The work was carried out on four different materials; styrene–butadiene rubber (SBR), ethylene–propylene–diene rubber (EPDM), plasticized PVC and low density polyethylene (details are given in the appendix). Only the first two materials are chemically cross-linked elastomers but the last two also exhibit rubberlike deformations by virtue of physical "cross-links" e.g. the crystalline regions in polyethylene.

All tests were carried out at 23° C but to obtain variations of $\mathcal{T}$, three different crack velocities were used for each material. Since local strain rates are controlled by the crack velocity, β and thus Φ are also sensitive to this variation.

2 Experimental investigations

2.1. Specimens

The two types of specimen used were cut from 2 mm thick compression moulded sheets of the materials. The first specimen was a normal tensile dumb-bell with a 6 mm wide gauge length for the determination of stress–strain and hysteresis data, and the second a parallel sided strip containing an edge crack positioned centrally to the specimen. These strips were 8 cm × 1 cm and the usual crack length c was 1 mm.

To facilitate strain distribution measurements, a grid was printed on to edge–crack specimens covering a region of about 1 cm^2 around the 1 mm crack. This was done by evaporating aluminium through a metal grid with 50 lines cm^{-1}.

2.2. Determination of $k_1(\epsilon_0)$

The function $k_1(\epsilon_0)$ was evaluated by the compliance method which is fully described elsewhere [2]. Parallel sided strips of the material in question, containing edge cracks of different lengths, were deformed in tension and their load–deflection curves recorded. The increase of compliance with crack length was converted into an apparent stored-energy change $-\mathrm{d}\mathcal{E}/\mathrm{d}c$ and the value of k_1 derived from the relation [1],

$$-\left.\frac{\mathrm{d}\mathcal{E}}{2h\mathrm{d}c}\right|_{\epsilon_0} = k_1(\epsilon_0)\, cW_0$$

where h is the sheet thickness. Note that constant ϵ_0 implies constant *load* conditions since ϵ_0 is the strain-at-infinity not the mean strain of the speci-

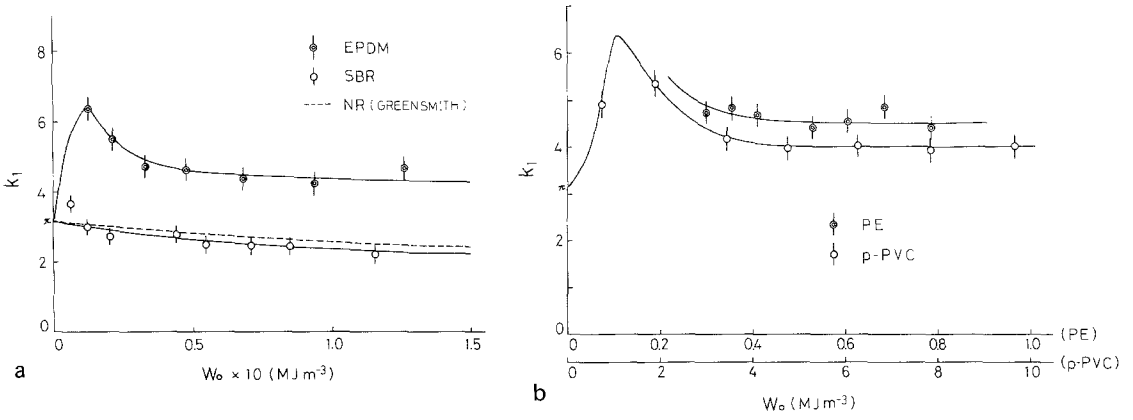

Figure 1 The function k_1 (W_0) for the four materials at 23° C; (a) for SBR and EPDM (b) for PE and p-PVC.

men. Also, since ϵ_0 and W_0 are uniquely related for a given material under fixed conditions of strain rate and temperature, it is possible and convenient to display k_1 as a function of W_0, $k_1(W_0)$, rather than ϵ_0. Results for $k_1(W_0)$ are shown in Fig. 1 for the four materials studied.

2.3. Measurement of crack velocity

To obtain accurate crack velocity data, referred to the unstrained state, the following procedure was adopted. Edge crack specimens were extended in an Instron testing machine to an overall extension ratio α_0 in a time t_1, held at α_0 for the time t_2 and returned to zero strain in time t_3. The total crack growth Δc during this cycle was then measured off the fracture surface. Keeping α_0, t_1 and t_3 constant, cycles were performed with varying t_2, and the crack velocity $\dot{c}$ at entension ratio α_0 obtained as the slope of a plot of Δc against t_2. This somewhat elaborate procedure is advisable because of the distortion of linear distances in the crack tip vicinity when the specimen is under strain.

The procedure was repeated for various values of α_0 for each material, keeping $c \simeq 1$ mm throughout. Typical results are shown in Fig. 2a for SBR and EPDM, and in Fig. 2b for PE and p-PVC.

2.4. Measurement of hysteresis ratio β

Stress–strain reversal loops were obtained in the positive strain and stress quadrant using dumb-bell

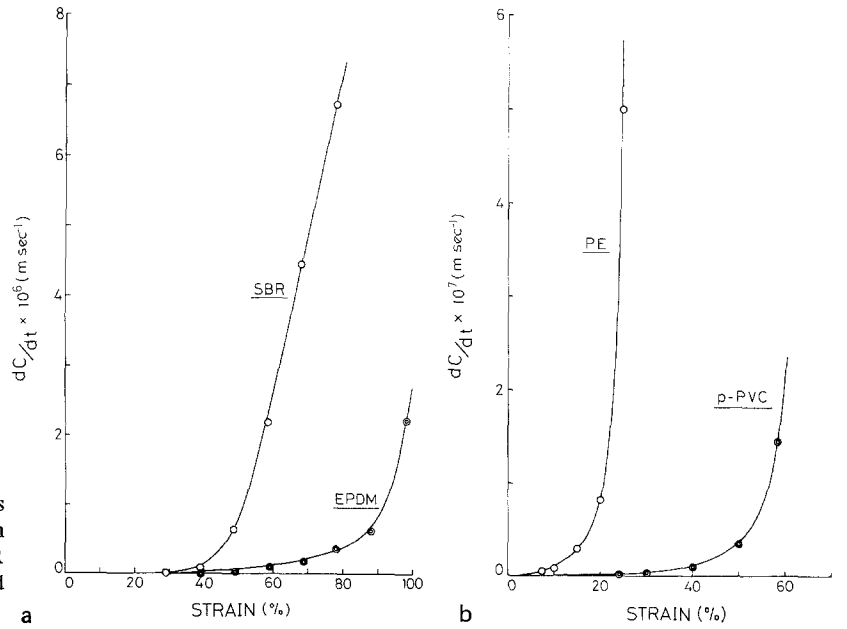

Figure 2 Crack velocities as functions of overall strain ratio α_0 at 23° C; (a) for SBR and EPDM (b) for PE and p-PVC.

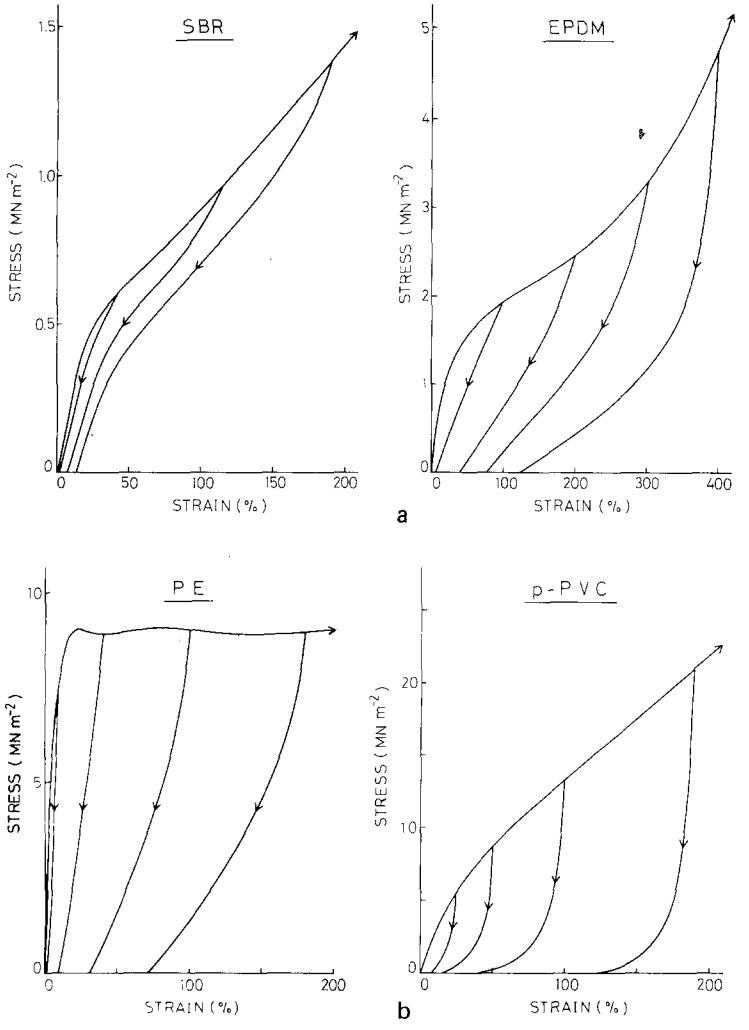

Figure 3 Typical hysteresis loops at 23° C; (a) for SBR and EPDM (b) for PE and p-PVC.

specimens and the Instron testing machine. The strain axis of the Instron chart was calibrated using bench marks in the gauge length in the normal way for highly extensible materials. Stress–strain loops of the form shown in Fig. 3 were obtained using a new specimen for each new strain level. The work was repeated for various straining rates and for all materials.

The input energy density W is given by the area under the loading curve up to a particular strain ϵ, and the recoverable energy density W_r by the corresponding area under the unloading curve. The hysteresis ratio is then given by

$$\beta(\epsilon, \dot{\epsilon}) = (W - W_r)/W \qquad (6)$$

Data for β are shown in Fig. 4 and as expected, β increases rapidly with strain and tends to increase with strain rate, though different materials behave differently with respect to the latter variable. The magnitude of β also varies greatly between materials, ranging from less than 20% for SBR to up to 90% for the less elastic solids.

2.5. Measurement of strain distribution

Crack propagation at known $\dot{c}$ was established by extending edge-crack specimens to a given α_0. The distorted grid around the (slowly) propagating crack was photographed for comparison with an earlier photograph of the unstrained specimen (see Fig. 5). Using the undeformed grid as a reference, the local extension ratios (α_x, α_y) along the X and Y axes of the grid were readily obtained and plotted as functions of the undistorted co-ordinates X, Y.

This defines the strain field, but since the principal axes of strain do not, in general, coincide with the X, Y grid lines [6], (α_x, α_y) are not principal strains and cannot be used directly to obtain the input energy density W at a point.

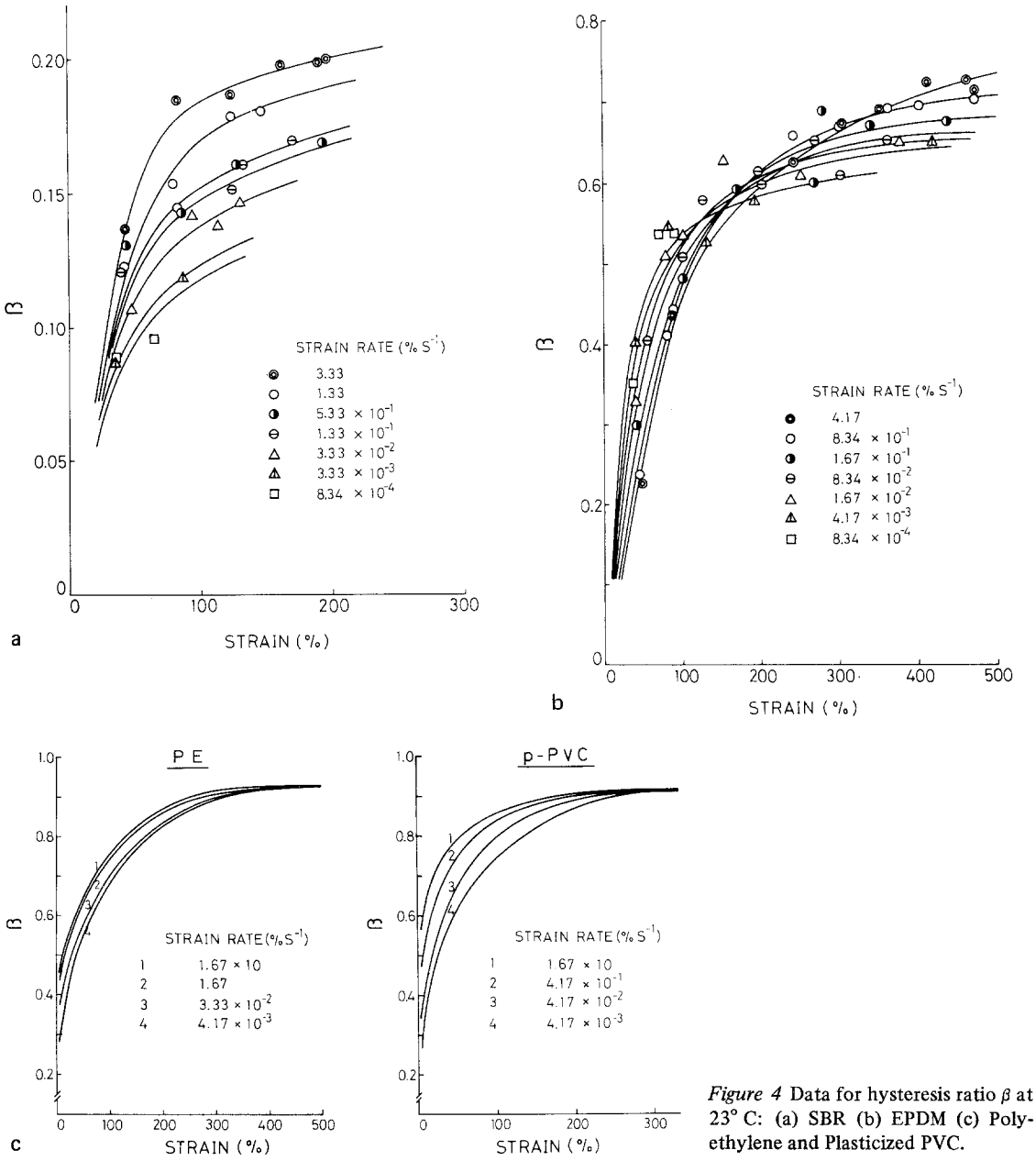

Figure 4 Data for hysteresis ratio β at 23° C: (a) SBR (b) EPDM (c) Polyethylene and Plasticized PVC.

To obtain the principal strains at a point required the following procedure. The distorted shape of OA′B′C′ of a selected grid square was redrawn and compared with a standard grid square OABC (see Fig. 6) at the correct orientation. The sides AB, BC of the undistorted grid were each divided into ten divisions by marks at (a_1, a_2 ... a_9) and (b_1, b_2 ... b_9). Similar divisions (a'_1, a'_2 ... a'_9) and (b'_1, b'_2 ... b'_9) were made along the sides of the distorted grid. A pair of mutually perpendicular lines (Ob_n, Ca_n) in the undistorted grid become (Ob'_n, $C'a'_n$) in the distorted grid. If the latter pair of lines remain perpendicular in spite of distortion, they are principal axes of strain and the principal extension ratios α_1 and α_2 are (Ob'_n/Ob_n) and (Ca'_n/Ca_n) respectively, assuming of course that the grid is sufficiently fine. Such pairs of lines are readily obtained by inspection and allow the construction of a map of principal strain directions (Fig. 7). Note that for highly deformable materials a line of principal strain is *not* a line which suffers no rotation during deformation as is the case for infinitesimal strain fields.

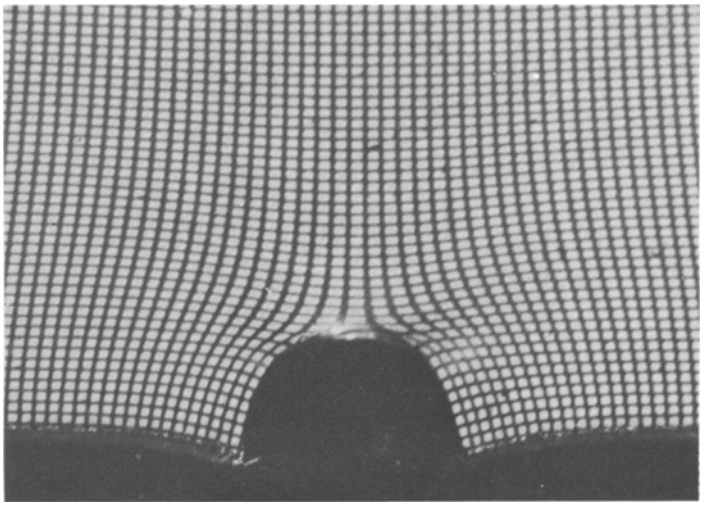

Figure 5 Strain field around propagating crack revealed by distorted grid.

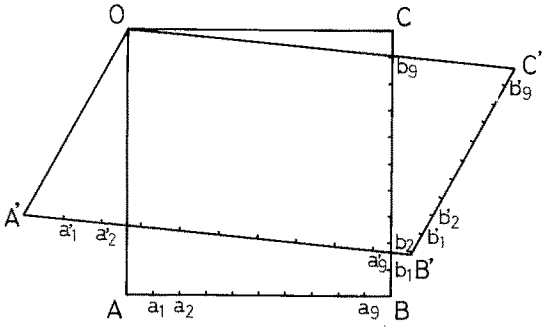

Figure 6 Derivation of principal strain ratios from distorted $X - Y$ grid.

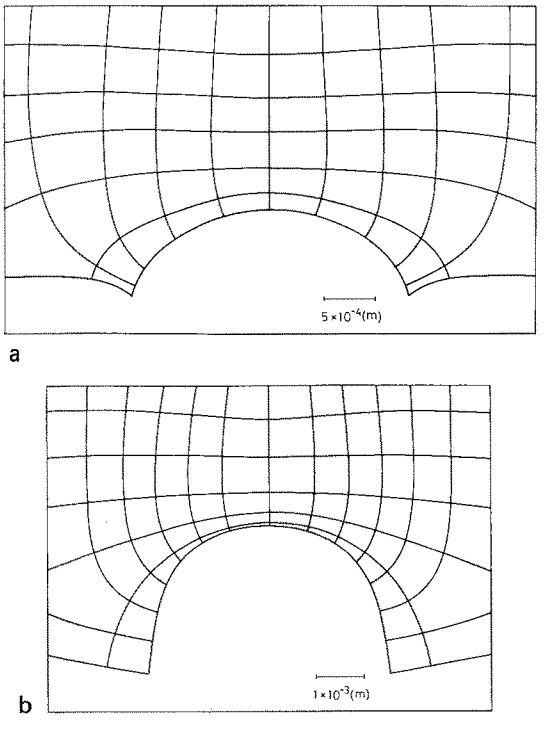

Figure 7 Typical map of principal strain directions; (a) for SBR at $\alpha_0 = 1.56$ (b) PE at $\alpha_0 = 1.26$.

2.6. Energy density distribution

The distribution of input energy density with respect to X, Y can be obtained from the strain distribution to a sufficient approximation for cross-linked elastomers and moderate strains by use of the theory of rubberlike elasticity which gives [7]

$$W = C_1[\alpha_1^2 + \alpha_2^2 + (\alpha_1\alpha_2)^{-2} - 3] \qquad (7)$$

assuming deformation at constant volume. This formula probably underestimates W by some 6% relative to the Mooney–Rivlin function involving two constants C_1 and C_2, but this error is offset by later approximations. The parameter C_1 is obtained from Equation 7 using simple extension data for which $\alpha_2 = \alpha_1^{-1/2}$. This data is given in Fig. 8 for SBR which shows a good linear fit in accordance with Equation 7.

For PVC and polyethylene, which cannot be expected to obey rubberlike elasticity theory, a rather different approach was necessary. For these materials stress–strain curves were obtained in simple extension and in pure shear ($\alpha_2 = 1$) the latter case being approximated by a sheet specimen held between long parallel grips whose initial separation was very much smaller than their length. Fig. 9 shows input energy density for the two modes of deformation for PE and PVC. Each

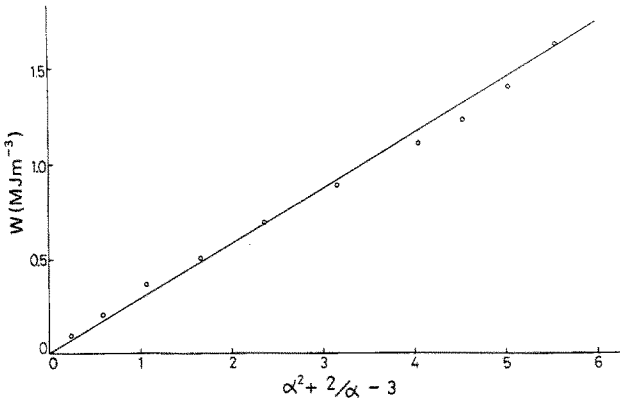

Figure 8 Derivation of C_1 for SBR at 23° C.

point on the simple extension curve represents a different α_2 value which is related to α_1 and the effective Poisson's ratio. A family of curves for fixed α_2 other than unity can then be generated by using the appropriate point on the simple-extension curve and the appropriate (positive or negative) intercept on the W axis for $\alpha_1 = 1$ inferred from the pure shear curve, and assuming that the family of curves generated by different constant α_2 values have the same shapes as that for $\alpha_2 = 1$. The broken lines in Fig. 9 show these constructions. Since the states of strain encountered around the crack are almost everywhere intermediate between simple extension and pure shear, and since $W(\alpha_1)$ differs by only 20% between the two states of strain, this somewhat crude construction probably gives $W(\alpha_1, \alpha_2)$ to an accuracy of a few percent.

Finally, therefore, it is possible to specify the input energy density W throughout the measured strain field and maps showing iso-energy contours are given in Fig. 10, by way of example, for SBR at $\alpha_2 = 1.56$ and PE at $\alpha_0 = 1.26$. This diagram also identifies the loci of maximum input energy density (broken lines) which in turn divide the strain field into regions which unload as the crack propagates (i.e. regions between the loci and the crack) and regions where W increases with propagation. The energy density distribution is always mapped on the unstrained co-ordinates, since only in this co-ordinate system is the sheet thickness constant with respect to X, Y.

2.7. The distribution of strain rate and β

The linear strain rate at a point is assumed to be given by

$$\frac{d\epsilon(P)}{dt} = \frac{d\epsilon(P)}{dY} \cdot \frac{dY}{dt} \tag{8}$$

$$\dot{\epsilon}(P) = -\left(\frac{d\epsilon(P)}{dY}\right) \dot{c} \tag{9}$$

where ϵ is the major principal strain. Thus the strain rate at all points in the strain field can be obtained from the strain distribution and the crack velocity. Given the input energy density W and the strain rate at a point, a value of β may then be assigned to that point.

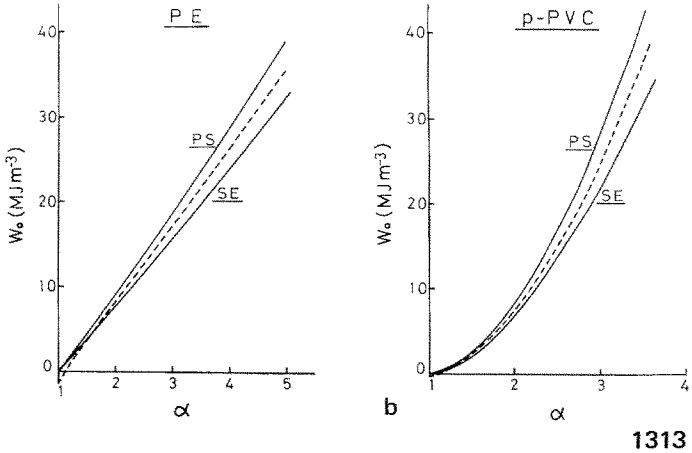

Figure 9 Input energy density as a function of α_1, α_2; (a) Polyethylene (b) plasticized PVC.

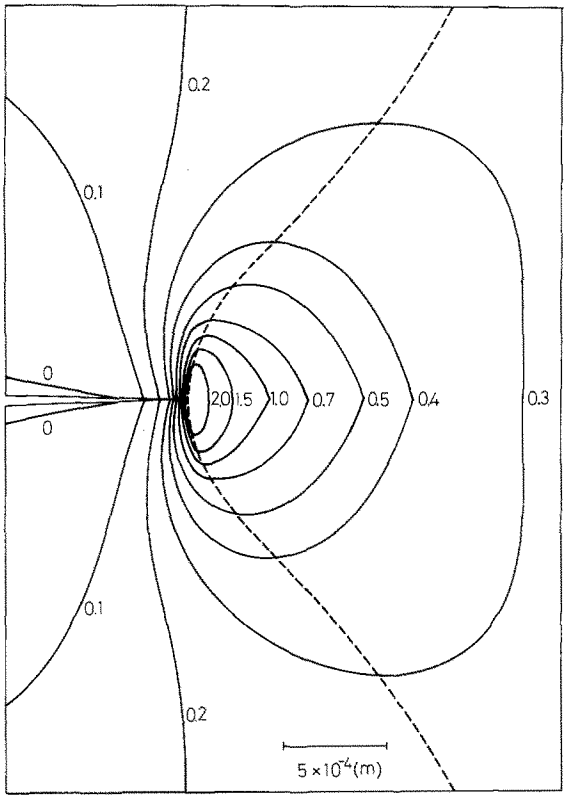

a

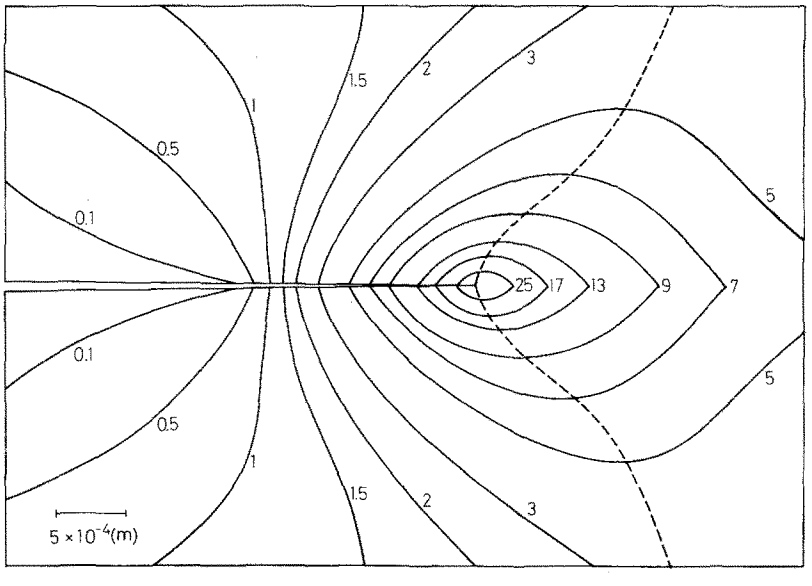

b

Figure 10 Iso-energy contours (energy density in MJ m^{-3}); (a) for SBR at $\alpha_0 = 1.56$ (b) for PE at $\alpha_0 = 1.26$. Unloading zones and loading zones separated by broken line.

3. Calculation of $\sum_{PU}$

Allowing $\delta x, \delta y \to 0$, we have from Equations 2–5

$$\tfrac{1}{2}\sum_{PU} \beta g \delta x \delta y = \frac{1}{W_0 c^2} \int_x^{PU} \int_y^{PU} \beta\left(X\frac{dW}{dX} + Y\frac{dW}{dY}\right) dY dX \quad (10)$$

$$\equiv \frac{1}{W_0 c^2}\left(\int_y R_x dY + \int_x R_y dX\right) \quad (11)$$

where

$$R_x \equiv \int_{PU} \beta X dW \quad (12)$$

$$R_y \equiv \int_{PU} \beta Y dW \quad (13)$$

To evaluate R_x, plots are made of energy density W as a function of the product βX for various values of Y, where X, Y are always referred to the undeformed grid. R_x is obtained by graphical integration of βX with respect to W over those ranges of X, Y for which unloading occurs if the crack propagates (see Fig. 10). Figs. 11 and 12 respectively show W versus βX and R_x versus Y for the case of SBR at $\alpha_0 = 1.56$.

In a similar manner R_y is obtained from plots of W versus βY (Fig. 13) and takes the form shown in Fig. 14 when plotted against X.

Graphical integration finally gives the terms in the brackets of Equation 11 which, for the case chosen (SBR at $\alpha_0 = 1.56$), assume the following values

$$\int_Y R_x dY = -1.75 \times 10^{-2}\ (\mathrm{J\,m^{-1}})$$

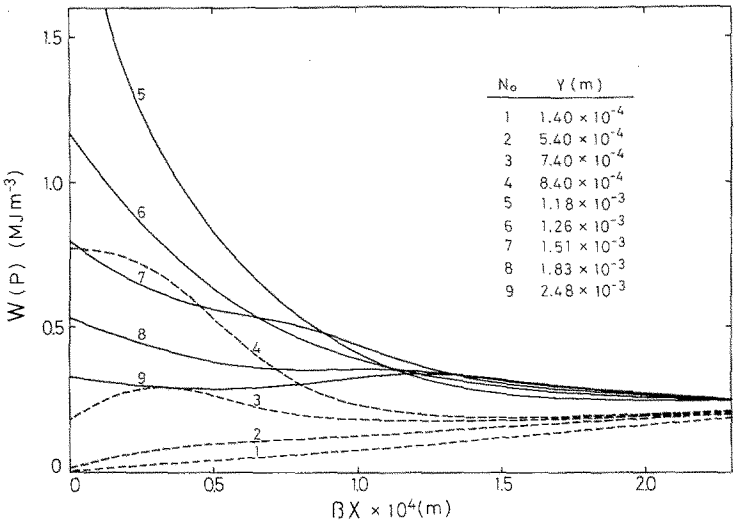

Figure 11 Plots of input energy density versus βX for SBR at $\alpha_0 = 1.56$ and at 23° C.

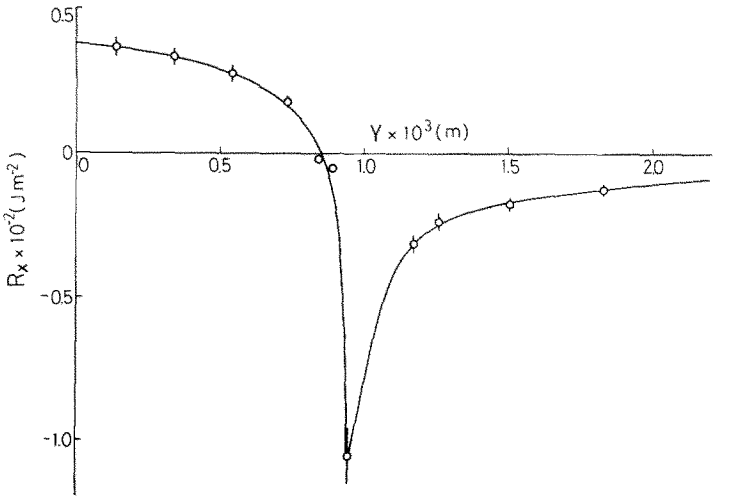

Figure 12 Plot of R_X versus Y for SBR at $\alpha_0 = 1.56$ and at 23° C.

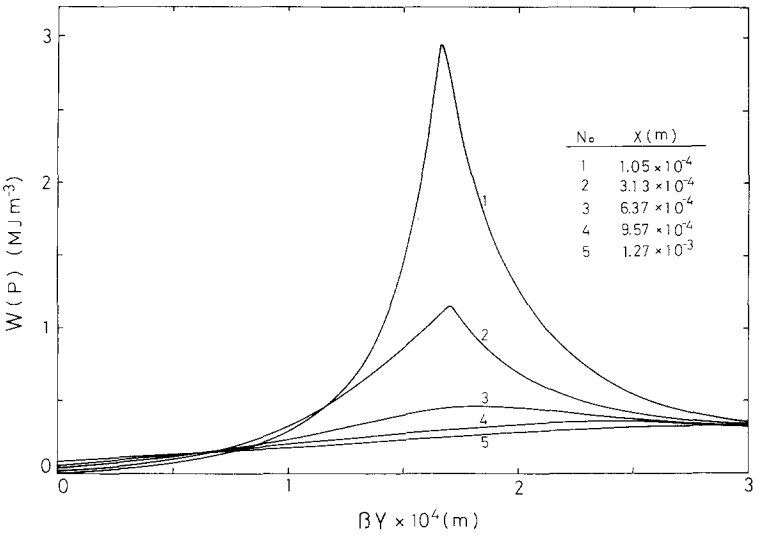

Figure 13 Input energy density versus βY for SBR at $\alpha_0 = 1.56$ and at 23° C.

$$\int_X R_y \mathrm{d}X = 3.80 \times 10^{-1}\ (\mathrm{J\,m^{-1}})$$

The former term is negative and small compared with the latter and neglecting it affects the value of Σ obtained from Equation 11 by only +5%. This effect is almost exactly offset by the probable 6% underestimate of $W(\alpha_1, \alpha_2)$ arising from use of the simpler statistical theory stored energy function for W, as mentioned earlier. In the results presented here, therefore, the term in R_x has been neglected throughout, and this greatly simplifies the task of evaluating Σ.

4. Calculation of $\mathcal{T}_0$

$\mathcal{T}_0$ is half the minimum energy required to break unit area of interatomic bonds across the fracture plane i.e. the surface energy of the solid on one definition. Lake and Thomas [5] have shown that for polymer networks this minimum energy can be calculated on the assumption that all the energy stored in the molecule between neighbouring cross-links is 'lost' to the elastic stress field if the molecule breaks between these cross-links. Their formula gives

$$\mathcal{T}_0 = \tfrac{1}{2}(\tfrac{3}{8})^{1/2}\,\gamma l U \xi \qquad (14)$$

where γ is a factor determined by the freedom of rotation about C–C bonds, l is the length of a monomer unit, U is the energy to rupture a C–C bond and $\xi = N\bar{n}^{3/2}$, where N is the number of chains per unit volume and $\bar{n}$ the number of monomer units in the network chain. (Note that $\mathcal{T}_0$ is half the quantity denoted T_0 by Lake and Thomas, the latter referring to both surfaces of the crack).

There is quite a wide margin of error in $\mathcal{T}_0$ calculated from Equation 14, and Lake and Thomas themselves give an alternative formula which gives values a factor of 2 greater. Fortunately it is possible to measure $\mathcal{T}_0$ values experi-

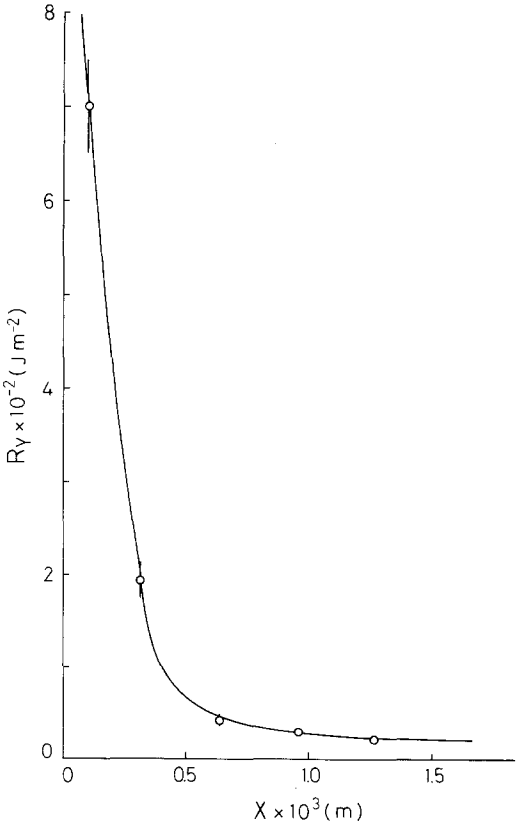

Figure 14 Plot of R_Y versus X for SBR at $\alpha_0 = 1.56$ and at 23° C.

TABLE I Experimental values for the parameter $\mathcal{T}_0$ for various cross-linked elastomers

Materials	$\mathcal{T}_0$ (J m^{-2})		Reference
	(in air)	(*in vacuo*)	
Natural rubber	10–20	33	Lake & Lindley [3]
Isomerized NR	35	–	
Synthetic *cis* PI	35	–	
Butadiene-styrene copolymer	30	–	
Butadiene-acrylonitrile copolymer	< 50	–	
Polychloroprene	35	–	
Butyl rubber	20	20	
Polybutadiene	20–50	–	Ahagon & Gent [9]
Styrene-butadiene copolymer	45	–	Andrews & Kinloch [4]

mentally for elastomers under certain circumstances, some examples being shown in Table I. The methods employed to measure $\mathcal{T}_0$ are discussed fully in the references to Table I, but include fatigue testing to vanishingly small crack growth rates and very slow tearing. Testing in vacuum instead of air increases $\mathcal{T}_0$ (for unsaturated polymers) by factors of up to 3 and some of the higher figures in Table I were obtained by the inclusion of antioxidants in the rubber.

The observed reduction of $\mathcal{T}_0$ by oxygen in very low rate tests used to gather the data of Table I) is significant when we come to consider the value of $\mathcal{T}_0$ appropriate to the present experiments where the time scale of crack propagation is much shorter. The appropriate values of $\mathcal{T}_0$ for inclusion in Equation 1 may well be higher than those quoted because the bond disruption energy U is not significantly reduced by oxygen attack on the short time-scale involved in normal tearing. It is difficult to estimate the magnitude of this effect but clearly the $\mathcal{T}_0$ value at the tearing rates used in the present work should be intermediate between the values in Table I and the corresponding *in vacuo* values, i.e. in the range 40 to 80 J m^{-2} for normal vulcanizates of NR and SBR protected by antioxidants.

Returning to the calculation of $\mathcal{T}_0$ we find that Lake and Thomas obtained values which were characteristically a factor of 2 to 3 smaller than the *in vacuo* experimental values for the appropriate vulcanizates. They attributed this discrepancy to inadequacies in the theory.

We have carried out calculations of $\mathcal{T}_0$ for the materials employed in the present work, using the parameters set out in Table II (for detailed justification of these values, see [8]). The resulting theoretical values for $\mathcal{T}_0$ are displayed in Table III which also includes previous slow-rate experimental data where available, and the experimental $\mathcal{T}_0$ values derived by the present study by an entirely different method i.e. by the use of Andrews' Equation 1 and 2 as discussed later.

In deriving theoretical $\mathcal{T}_0$ values for the uncross-linked systems polyethylene and plasticized PVC effective values for the Mooney–Rivlin constants C_1 and C_2 were derived from Mooney–Rivlin plots and averaged over their rate-dependence. These values are thus not determined with any great accuracy as indicated by the following values and error bands.

	C_1 (MN m^{-2})	C_2 (MN m^{-2})
plasticized PVC	0.55 ± 0.35	4.1 ± 1.9
polyethylene	0.15 ± 0.05	3.8 ± 0.2

5. Synthesis of results

In the results reported above, all the components of Equations 1 and 2 have been separately

TABLE II

Parameters	SBR	EPDM	PE	PVC
$l \times 10^{10}$ (m)	5.15	3.32	2.50	2.50
$m \times 10^{25}$ (N)	12.6	6.79	4.57	10.2
γ	1.54	1.83	1.83	2.77
$U \times 10^{19}$ (J)	12.8	8.78	6.60	6.60
θ (K)	296	296	296	296
η	1.15	1.15	–	–
$\rho \times 10^{-4}$ (N m^{-3})	0.901	0.871	0.922	0.987
$M \times 10^{23}$ (N)	32.7	16.3	–	7.35
$\nu' \times 10^{-25}$ (m^{-3})	1.93	1.93	–	–
$C_1 \times 10$ (MN m^{-2})	2.0	2.0	1.5 ± 0.5	5.5 ± 3.5

TABLE III Values of $\mathcal{T}_0$ (J m^{-2})

Material	Theoretical	Experimental (this work)	Experimental (other work)
			(*in vacuo*)*
NR	10 ~ 14	–	20 [3]*
			30 [3]*
SBR	16	65 ± 15	30 [3]
			45 [4]
EPDM	18	65 ± 15	–
p-PVC	15 ± 5	100 ± 50	–
PE	31 ± 6	200 ± 100	–

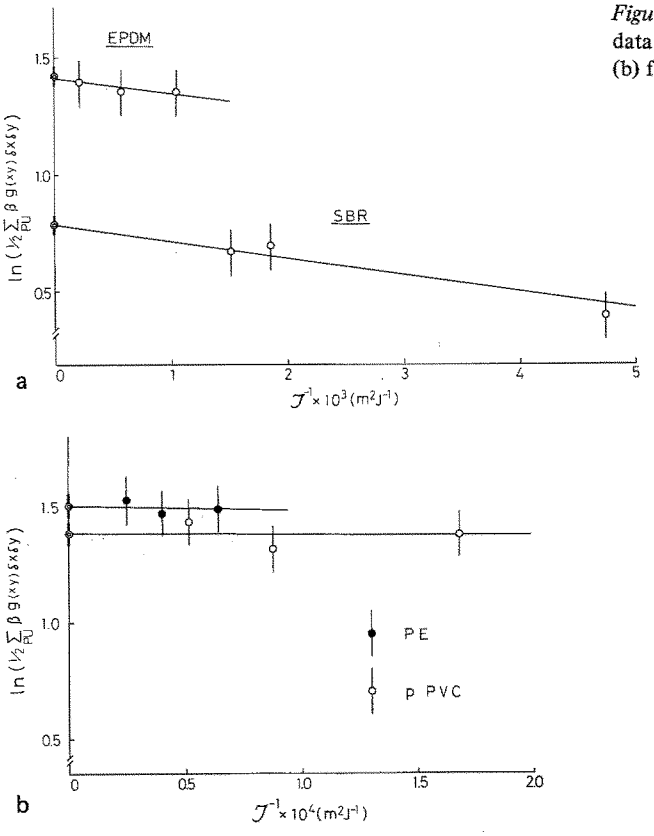

Figure 15 Plots showing agreement of experimental data points with Equation 17; (a) for SBR and EPDM (b) for PE and PVC.

evaluated and it remains to compare the directly measured values of $\mathcal{J}$ with those derived using the equation. Because, however, the values of $\mathcal{J}_0$ are somewhat uncertain within a factor of about 2, it serves our purposes better to treat $\mathcal{J}_0$ as the unknown in Equation 1, thus deducing a value for comparison with the data given in Section 4 of this paper.

To do this we rearrange Equations 1 and 2 thus, using Σ as a 'shorthand' for the summation in Equation 2;

$$\frac{\mathcal{J}}{\mathcal{J}_0} = \frac{k_1}{k_1 - \frac{1}{2}\Sigma} \tag{15}$$

$$k_1(1 - \mathcal{J}_0/\mathcal{J}) = \tfrac{1}{2}\Sigma \tag{16}$$

Since $\mathcal{J}_0/\mathcal{J} \ll 1$ for most conditions, we take natural logarithms to get

$$\ln k_1 - \mathcal{J}_0/\mathcal{J} = \ln \tfrac{1}{2}\Sigma \tag{17}$$

so that a graph of $\ln \frac{1}{2}\Sigma$ against $\mathcal{J}^{-1}$ should give a straight line of negative slope $-\mathcal{J}_0$ with an intercept of $\ln k_1$ as $\mathcal{J}^{-1} \to 0$. For each material $\mathcal{J}$ was measured directly at three different crack velocities and the corresponding k_1 and summation terms were evaluated as discussed above. Thus for each material we can plot $\ln k_1$ at $\mathcal{J}^{-1} = 0$ and three separate points of $\mathcal{J}^{-1}$ against $\ln \frac{1}{2}\Sigma$. These plots are shown in Fig. 15, where the error bars on the points reflect the uncertainties in evaluating Σ.

It is clear that the theoretical relationship of Equation 17 represents the data well, especially for the cross-linked materials SBR and EPDM. The small negative slope of the best straight line through the points can be estimated reasonably accurately for SBR and EPDM, though only with considerable error in the case of PE and p-PVC. These slopes should, of course, equal $\mathcal{J}_0$ and their values are compared with theoretical and previous experimental data in Table III.

The agreement is very satisfactory, especially bearing in mind the comments made earlier about the rather higher $\mathcal{J}_0$ values to be expected from non-oxidative conditions. Certainly the linearity and negative slopes in Fig. 15, together with the good order-of-magnitude results for $\mathcal{J}_0$, seem to

TABLE IV Details of materials used

Abbreviation	Name	Content (by weight)	Molecular weight
SBR	Styrene Butadiene Rubber	$\frac{S}{B} = \frac{70}{30}$	2.0×10^5
EPDM	Ethylene Propylene Diene Rubber	$\frac{E}{P} = \frac{67}{33}$	1.0×10^5
p-PVC	Plasticized Polyvinyl Chloride	PVC/plasticizer $= \frac{67}{33}$ Plasticizer (di-octyl phthalate) (di-alphanyl phthalate)	4.5×10^4
PE	low density Polyethylene	d = 0.922	

provide excellent confirmation of Equations 1 and 2, and thus of the generalized theory proposed by Andrews.

TABLE V The compounding recipes and cures of vulcanizates

Composition (parts by wt)	SBR	EPDM
Rubber	100	100
Sulphur	4	0.1
Diphenyl guanadine	3	–
Dicumyl peroxide	–	1
Zinc oxide	5	–
Stearic acid	2	–
Phenyl-2-naphthylamine	1	–
Cure temperature (K)	418	423
Cure time (sec)	3.3×10^3	2.4×10^3

References

1. E. H. ANDREWS, *J. Mater. Sci.* 9 (1974) 887.
2. E. H. ANDREWS and E. W. BILLINGTON, *ibid* **11** (1976) 1354.
3. G. J. LAKE and P. B. LINDLEY, *J. Appl. Polym. Sci.* 9 (1965) 1233.
4. E. H. ANDREWS and A. J. KINLOCH, *Proc. Roy. Soc. London* **A.332** (1973) 385.
5. G. J. LAKE and A. G. THOMAS, *ibid.* **A.300** (1967) 108.
6. E. H. ANDREWS, *Proc. Phys. Soc.* 77 (1961) 483.
7. L. R. G. TRELOAR, "The physics of rubber elasticity" 2nd Ed. (Oxford University Press, Oxford, 1958).
8. Y. FUKAHORI, Ph.D. Thesis (University of London) 1976.
9. A. AHAGON and A. N. GENT, *J. Polym. Sci. (Polym. Phys. Ed.)* **13** (1975) 1903.

Received 30 November and accepted 16 December 1976.